

Article

Dissolution Behavior of Alumina-Based Inclusions in $\text{CaF}_2\text{-Al}_2\text{O}_3\text{-CaO-MgO-SiO}_2$ Slag Used for the Electroslag Metallurgy Process

Yanwu Dong *, Zhouhua Jiang and Ang Yu

School of Metallurgy, Northeastern University, Shenyang 110819, China; jiangzh@smm.neu.edu.cn (Z.J.); biam_yuang@foxmail.com (A.Y.)

* Correspondence: dongyw@smm.neu.edu.cn; Tel.: +86-24-8369-1689

Academic Editor: Alexandru Mihai Grumezescu

Received: 23 September 2016; Accepted: 7 November 2016; Published: 9 November 2016

Abstract: Removal of non-metallic inclusions to CaF_2 -based slag is one of the most important functions of electroslag remelting. In this work, the dissolution behavior for alumina-based inclusions in $\text{CaF}_2\text{-Al}_2\text{O}_3\text{-CaO-MgO-SiO}_2$ slag has been investigated. Results indicate that the diffusion or permeability capacity of slag components into alumina particles is F^- , Ca^{2+} , Si^{4+} , Mg^{2+} , from strongest to weakest, for $\text{CaF}_2\text{-Al}_2\text{O}_3\text{-CaO-MgO-SiO}_2$ slag. Alumina inclusions react with F^- in liquid slag at first and then react with CaO to form $x\text{CaO-yAl}_2\text{O}_3$ system. Subsequently, MgO substitutes for CaO to form a $\text{MgO-Al}_2\text{O}_3$ system layer surrounding the other product and reactant, and then enters the liquid slag. CaF_2 can improve the dissolution capacity of slag to alumina inclusions. A complex region was formed between alumina-based particles and the slag, with different areas dominated by CaF_2 , $\text{CaO-Al}_2\text{O}_3$, CaO-SiO_2 and $\text{MgO-Al}_2\text{O}_3$. The dissolution process of alumina particles in slag is different from the formation of compound inclusions originated from the Al-O deoxidization reaction.

Keywords: electroslag metallurgy; alumina inclusions; fluoride containing slag; dissolution mechanism

1. Introduction

Electroslag remelting has been widely used for the manufacture of high quality steel and alloys. This process creates a sound product with a homogeneous compositions and a low concentration of very small inclusions [1]. As is well known, the removal of non-metallic inclusions from the consumable electrode is one of the most important characteristics for the electroslag remelting process. The process of removing inclusions mainly happens at the tip of the electrode, and involves the absorption and dissolution of inclusions in fluoride-containing slag [2,3]. Although the removal process of inclusions has been studied during electroslag remelting, the mechanism for their absorption and dissolution in slag is not clear. Alumina-based inclusions are typically the most common inclusions in Al-killed steel [4,5]. Therefore, the investigation of the dissolution of alumina inclusions in fluoride slag is very significant.

Many studies of the dissolution behavior of alumina inclusions in slag systems [6–9] including $\text{CaO-Al}_2\text{O}_3\text{-SiO}_2$ melts [7,8], $\text{CaO-Al}_2\text{O}_3\text{-SiO}_2\text{-MgO}$ [9], and $\text{Al}_2\text{O}_3\text{-CaO-FeO}_x\text{-SiO}_2$ [10] have been carried out. They had found that the alumina dissolution rate was affected by the rotation speed of the rod, the temperature and the viscosity of the slag [6,11]. Yan et al. [9] found that the rate-limiting step of Al_2O_3 dissolution is mass transfer through the boundary layer and established a range of effective diffusion coefficients. Bui et al. [12] investigated the effect of the alumina content and solid phase in molten flux on the dissolution of alumina. In addition, they indicated that an intermediate compound played an important role in alumina dissolution in slag. Park et al. [8] investigated the interfacial reaction between alumina refractory and $\text{CaO-CaF}_2\text{-SiO}_2\text{-Al}_2\text{O}_3\text{-MgO-MnO}$ slag and the impact of the CaO/SiO_2 ratio on the spinel solution.

Some investigations [13–15] have studied alumina solubility and diffusion in fluoride electrolytes. Frazer et al. [13] studied alumina particle solubility and diffusion behavior in NaF-AlF₃ and NaF-AlF₃-CaF₂ systems and estimated the diffusion coefficient. Yang et al. [15] measured alumina solubility in a range of KF-AlF₃-based low-temperature electrolyte systems.

In recent years, Monaghan and Chen [16], Fox and Valdez et al. [17], Verhaeghe and Liu et al. [18], Liu and Verhaeghe et al. [19], and Orrling and Sridhar et al. [20] employed laser scanning confocal microscopy (CSLM) to investigate the dissolution of inclusions in slag. CSLM enables the in-situ observation of the dissolution of inclusions. A transparent liquid slag is an important requirement for these types of investigations; however, most fluoride slags are not transparent. Therefore, CSLM cannot be used to study the dissolution of inclusions in most fluoride-containing slags. Though Sridhar et al. [21] and Yu et al. [12] investigated the behavior of alumina in Na₂O-CaO-Al₂O₃-SiO₂-CaF₂, it has a low fluoride content in the slag and the situation is different for fluoride-containing slags. Examples cannot be found in the literature for the dissolution of alumina inclusions in the fluoride-containing slag used in the electroslag remelting process. The dissolution/removal/modification of inclusions exists during electroslag remelting. However, dissolution is the first process, which is the important premise of removal and modification. Therefore, in this paper, the absorption and dissolution mechanisms of alumina inclusions in fluoride-containing slag have been investigated.

2. Materials and Methods

The experiment has been carried out using a resistance furnace (Ferrous Metallurgy Institute of Northeastern University, Shenyang, China) as shown in Figure 1. The heating unit is made of molybdenum disilicide. B-type thermocouple has been adopted for measuring the furnace temperature.

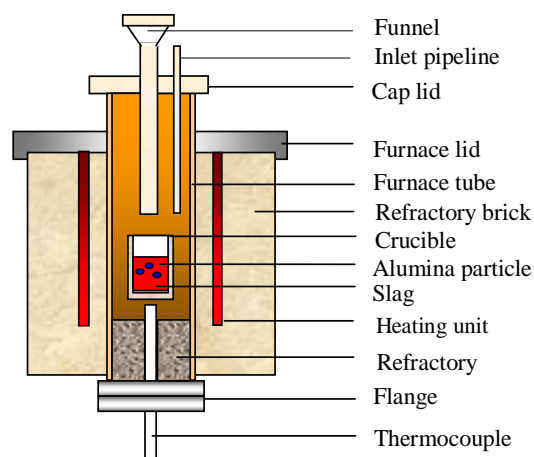


Figure 1. Schematic of experimental apparatus.

The material preparations before experiment are as follows. The bulk slag materials used in the experiment are composed of analytical reagents and were weighed using a high-precision electronic balance. The principal component content for each slag material is larger than 98.5%. The particle size is close to 0.15 mm. Slags charged in an alumina crucible were calcined at 1123 K for 4 h after thoroughly mixing in an agate mortar. The alumina crucible was then stored in a desiccator before the experiment. Experiments were carried out with two kinds of slag mixtures, including 50%CaF₂-20%Al₂O₃-20%CaO-5%MgO-5%SiO₂ (Slag S1) and 70%CaF₂-30%Al₂O₃ (Slag S2). The dimensions of alumina-based particle are 600–800 μm. Most alumina particles were subspheroidal in shape. X-ray diffraction (XRD) was used to analyze the phase components in the alumina-based as shown in Figure 2. In this example, the amount of Al₂O₃ is about 87.3% according to the XRD analysis. The other phases present are 8.5% CaAl₁₂O₁₉, 3.57% MgAl₂O₄ and 1.4% SiO₂, respectively.

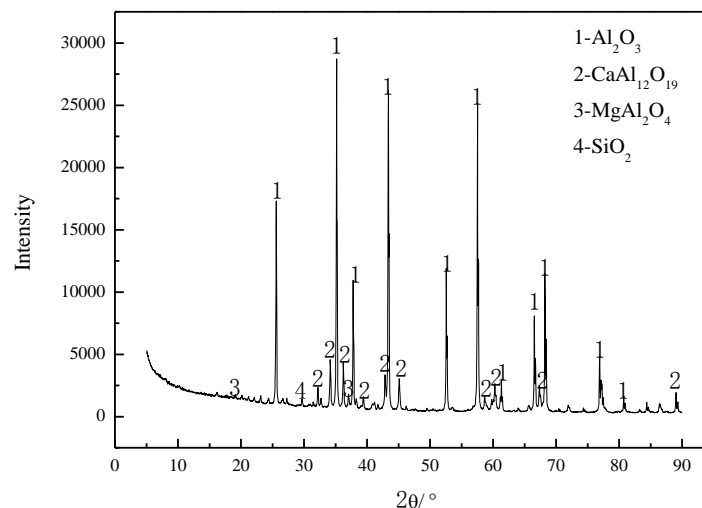


Figure 2. XRD analysis of alumina particle.

The detailed experiment was carried out according to the following procedure. At first, slag about 400 g in weight surrounded by a 0.3-mm-thick molybdenum film from the side and bottom was placed into a graphite crucible. Graphite crucible is 40 mm and 70 mm in inner diameter and height. The power was switched on after the graphite crucible had been placed in the furnace chamber. The furnace was heated to 1823 K at a rate of 6 K/min and then kept this temperature for 10 min. Then, about 15 g of the alumina-based particle were introduced into the liquid slag pool through hollow alumina tube of 20 mm in inner diameter as shown in Figure 1. After 10 s from alumina-based particle addition, an alumina crucible tied on a long molybdenum wire was introduced into liquid slag and then slag specimen was taken from the liquid slag pool. Immediately, the liquid slag in alumina crucible was quenched on a large steel block, on which had a cylindrical recess to keep the slag cylindrical. And then more specimens were taken from the liquid slag pool in order to investigate the solubility situation of alumina-based inclusion in slag. The argon with the 99.99% in purity, used as the shielding gas, was introduced into the chamber at 3 L/min by inlet pipeline from the top when the chamber temperature rose up to 573 K. The shielding gas was kept this rate until the experiment had been finished.

3. Results and Discussion

3.1. Characteristics of Alumina-Based Inclusions in Slag

The slag specimens obtained in the experiment were then ground and polished using standard metallography procedures. Some alumina-based inclusions were found in the slag specimens. Figure 3a shows the morphology of an alumina particle in solidified slag. It can be seen that the alumina particles do not dissolve completely. The color of the bulk slag and alumina particle is obviously different as observed by SEM. A clear boundary between the inclusion and slag can be observed due to different chemical compositions.

The white line of dashes in Figure 3a, a typical dissolution boundary between the inclusion and slag S1, has been enlarged in Figure 3b. The yellow line in Figure 3b is an obvious transition region, which is different in color from the other part. The characteristics of the boundary layer are similar for other particles found in slag specimens. Moreover, the inclusion particle dissolves with the duration of the reaction time and the boundary layer shifts to the inner part of the particle by analyzing the slag specimens at different times.

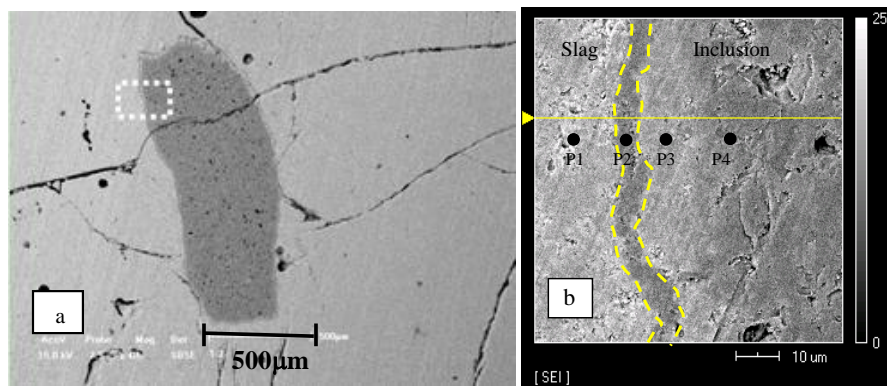


Figure 3. Results of (a) Typical morphology of alumina particle in slag S1 by SEM-SBSE and (b) line-scanning image of boundary layer.

The compositions of four positions in Figure 3b are listed in Table 1. It can be seen from the results that point P1 represents the bulk slag and point P4 is the inclusion body. Points P2 and P3 are in the boundary layer between the bulk slag and alumina-based particle. A higher Mg concentration exists at point P2, which may be due to the diffusion of Mg^{2+} in slag from the liquid slag to the alumina particle. High contents of Mg, Al and O at point P2 may be attributed to the formation of the $MgO-Al_2O_3$ system.

Table 1. Energy dispersive spectrometer (EDS) results of different points in specimen.

Element	Atom (%)			
	P1	P2	P3	P4
O	12.5	44.2	38.6	45.5
F	31.4	-	9.8	-
Mg	3.0	16.1	0.7	1.0
Al	8.6	37.3	26.4	50.4
Si	0.5	0.4	5.0	0.5
Ca	4.1	2.0	19.6	2.6

Line scanning has been done in order to investigate the dissolution mechanism of alumina inclusions in fluoride-containing slag as shown in Figure 4. The regions b, c, d and e are proposed as the dissolution boundary because of the rapid decrease or increase in F, Ca, O and Al. This proves that inclusion dissolution and ion diffusion in liquid slag occur simultaneously.

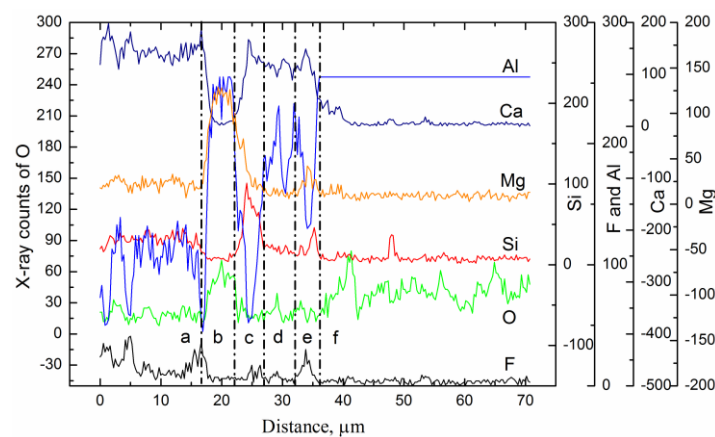


Figure 4. Line-scanning image of boundary layer of alumina particle and solid slag in slag S1.

More slag samples at different times were analyzed. Figure 5 shows one of the results after about 20 s of the addition of particle, which is similar to the results in Figure 4.

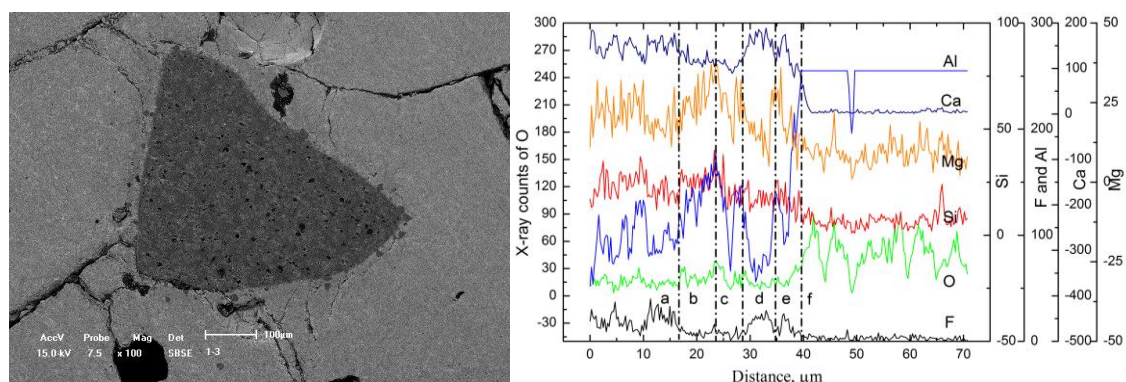
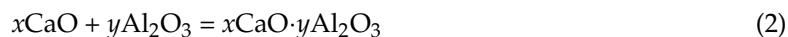


Figure 5. Morphology of alumina particle at another time in slag S1 by SEM-SBSE and line-scanning image of boundary layer.

3.2. Dissolution Behavior of Alumina Inclusions in Slag

It can be seen from Figures 4 and 5 that region *f* can be regarded as the inclusion body because of the constant Al content and lower F, Ca, Mg and Si levels. Region *a* is the bulk slag. Region *e* is the innermost reaction layer, in which higher F and Ca have been revealed. It indicates that the diffusion or penetration rate of Ca^{2+} and F^- toward the inclusion is faster than other components in the liquid slag. It can be inferred from the results obtained in Figures 3–5 that the following reaction has happened in this region.



The reaction product of Reaction (2) could then react with the alumina inclusion to form a $\text{CaO-Al}_2\text{O}_3$ system, as can be proved by the $\text{CaF}_2\text{-Al}_2\text{O}_3$ binary phase diagram. The molar ratio of CaO and Al_2O_3 mainly depends on the content of each component, which can also be clarified by the $\text{CaO-Al}_2\text{O}_3$ phase diagram as shown in Figure 6 [22].

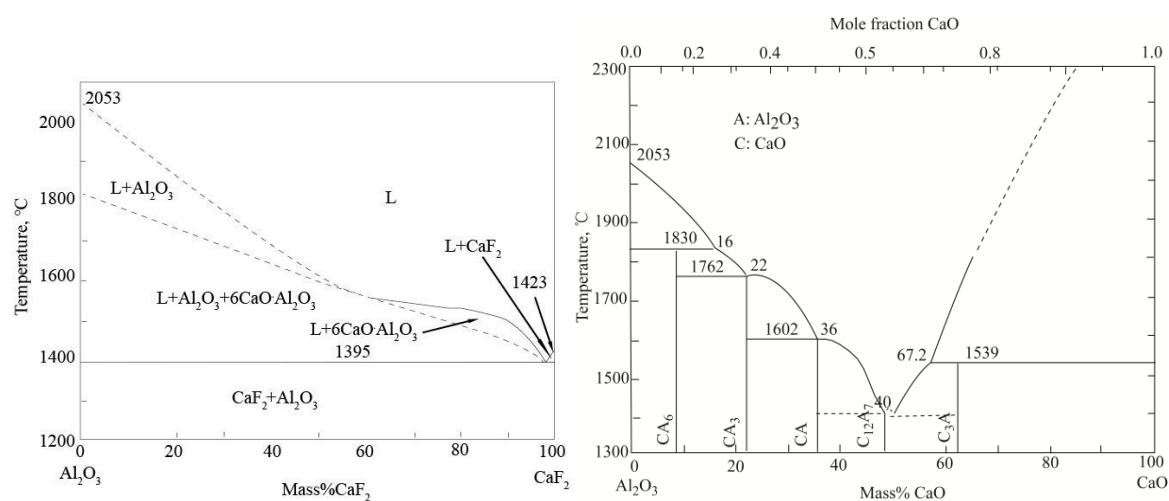


Figure 6. Binary phase diagram of $\text{CaF}_2\text{-Al}_2\text{O}_3$ and $\text{CaO-Al}_2\text{O}_3$.

In addition, the existence of F^- can improve the slag dissolution capacity to non-metallic inclusions, as can be proved by the findings of Cho and Fan [23]. They investigated the diffusion

dissolution of alumina in various steelmaking slags. The addition of CaF_2 in steelmaking slag can improve the dissolution rate of alumina particles in slag [23,24].

Higher Al and Ca but lower F, Mg and Si have been obtained for region d, implying that calcium aluminates could be present. The main component in region b is the $\text{MgO}\cdot\text{Al}_2\text{O}_3$ system; in addition, there is a small fraction of $\text{CaO}\cdot\text{Al}_2\text{O}_3$ spinel. The following reactions maybe happen from region c to region b.



Region c appears to be a transition region between the calcium aluminate-dominated region d and the spinel-dominated region b. Within region c there is an additional trend of an increase of the calcium and silicon levels, with a corresponding drop in aluminum, implying the formation of calcium silicates.

However, it is very complex for region c, in which the change trend is similar for Ca and Si, which first increase and then decrease. Al decreases first and then increases. It can be only inferred that $\text{CA}_6(\text{CaO}\cdot 6\text{Al}_2\text{O}_3)$, $\text{CA}_2(\text{CaO}\cdot 2\text{Al}_2\text{O}_3)$, $\text{CA}(\text{CaO}\cdot\text{Al}_2\text{O}_3)$, $\text{C}_{12}\text{A}_7(12\text{CaO}\cdot 7\text{Al}_2\text{O}_3)$ and $\text{C}_3\text{A}(3\text{CaO}\cdot\text{Al}_2\text{O}_3)$ may be present [22]. The content of CaO decreases; in contrast, Al_2O_3 increases at the same time in region c from the alumina particle to bulk slag direction. The reaction can be expressed by Reaction (2).

Results show only an increase in the MgO level in region b, with the level in other regions not going above the bulk slag levels. The present results indicate that an alumina inclusion will initially be attacked by calcium fluoride-based slag. For the experimental time used, complex behavior was observed in the region between the bulk alumina particle and the slag. After the initial attack area, there were regions dominated by calcium aluminates, calcium silicates and spinel, indicating a progression of reactions.

This behavior is different from that in conventional steelmaking, with alumina inclusions generated by Al deoxidation reacting with MgO to form $\text{MgO}\cdot\text{Al}_2\text{O}_3$ at first, and then the Ca element substitution for the Mg element in $\text{MgO}\cdot\text{Al}_2\text{O}_3$ inclusions to form $\text{CaO}\cdot\text{Al}_2\text{O}_3$ outside of the $\text{MgO}\cdot\text{Al}_2\text{O}_3$ core. The dissolution mechanism of alumina inclusions in $\text{CaF}_2\text{-Al}_2\text{O}_3\text{-CaO-MgO-SiO}_2$ slag can be illustrated as in Figure 7.

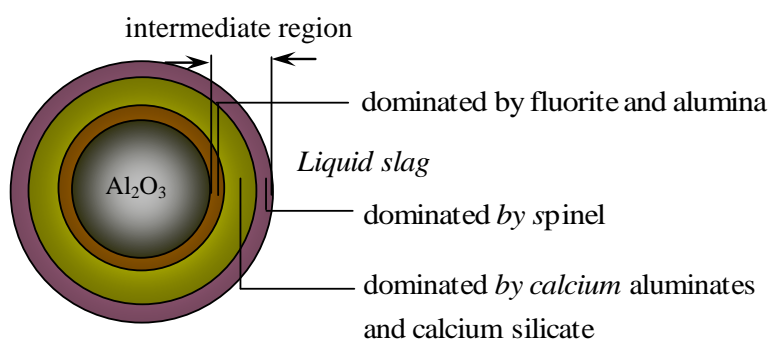


Figure 7. Dissolution mechanism of alumina inclusions in $\text{CaF}_2\text{-Al}_2\text{O}_3\text{-CaO-MgO-SiO}_2$ slag.

Figure 8 shows a SEM-SE image of the dissolution boundary between the inclusion and slag S2 as well as the line-scanning results of the boundary layer by SEM-SBSE. It can be seen that the color of the bulk slag and alumina particles is obviously different and the boundary is very clear. Similar results have been obtained, but it is easier than the dissolution of inclusions in slag S1. Only $\text{CaO}\cdot 6\text{Al}_2\text{O}_3$ exists in the dissolution process, which is from Reactions (1) and (2) because enough Al and less Ca exist in this region for slag S2. It can further illustrate that the resource of Si in region c of Figure 4 is from the diffusion of SiO_2 from the slag into the inclusions instead of the SiO_2 in the inclusions itself because no Si has been found in Figure 8, based on the same alumina inclusion particles in the experiment.

The dissolution behavior of alumina inclusions in $\text{CaF}_2\text{-Al}_2\text{O}_3$ slag should be very easy to study. Only Reactions (1) and (2) have happened because the components are only CaF_2 and Al_2O_3 in the slag.

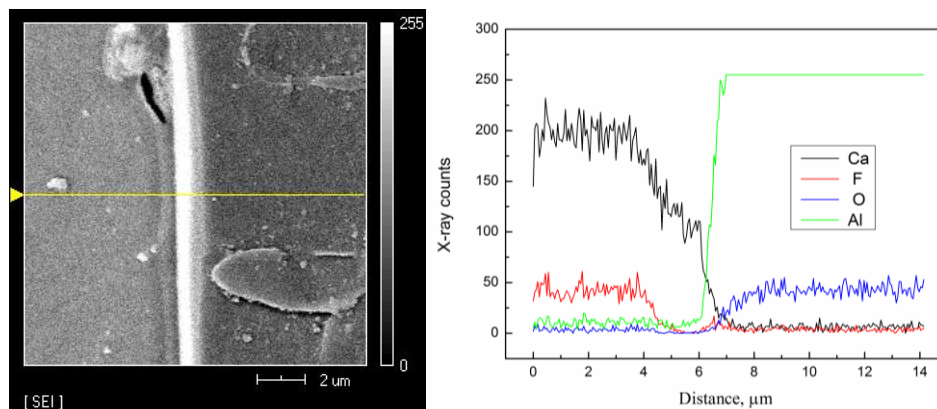


Figure 8. SEM-SE image of the dissolution boundary between the inclusion and slag S2 as well as line-scanning results of the boundary layer by SEM-SBSE.

4. Conclusions

The dissolution mechanism of alumina inclusions in $\text{CaF}_2\text{-Al}_2\text{O}_3\text{-CaO-MgO-SiO}_2$ slag has been investigated. The following conclusions can be drawn:

- (1) The diffusion capacity of ions in liquid slag into alumina particle is F^- , Ca^{2+} , Si^{4+} , Mg^{2+} , from strongest to weakest, for $\text{CaF}_2\text{-Al}_2\text{O}_3\text{-CaO-MgO-SiO}_2$ slag.
- (2) Alumina inclusions react with F^- to form AlF_3 at first, and then react with CaO to form $x\text{CaO}\cdot y\text{Al}_2\text{O}_3$ system inclusions. Subsequently, MgO substitutes for CaO to form a $\text{MgO-Al}_2\text{O}_3$ system layer surrounding the other product and reactant, and then enters the liquid slag.

Acknowledgments: This project supported by Fundamental Research Funds for the Central University of China with the grant No. 150202003. Also, this project supported by the Joint Research Fund of the National Nature Science Foundation of China and the Baosteel Group Corporation with the grant No. U1360103 and is supported by the National Nature Science Foundation of China with the grant No. 51274266.

Author Contributions: Yanwu Dong and Zhouhua Jiang conceived and designed the experiments; Aang Yu performed the experiments; Yanwu Dong and Ang Yu analyzed the data. Yanwu Dong wrote the paper with the support of Zhouhua Jiang.

Conflicts of Interest: The authors declare no conflict of interest.

References

1. Mitchell, A. Solidification in remelting processes. *Mater. Sci. Eng. A* **2005**, *413–414*, 10–18. [[CrossRef](#)]
2. Jiang, Z.H. *Physical Chemistry and Transmission Phenomena during Electroslag Metallurgy*, 1st ed.; Northeastern University Press: Shenyang, China, 2000; pp. 8–15.
3. Li, Z.B. *Electroslag Casing*, 1st ed.; National Defense Industry Press: Beijing, China, 1979; pp. 17–24.
4. Mapelli, C. Control and engineering of non-metallic inclusions belonging to $x\text{SiO}_2\cdot y\text{CaO}\cdot z\text{Al}_2\text{O}_3$ system in Ca-treated, Al-killed and Al-Si-killed steel. *Steel Res. Int.* **2006**, *77*, 462–471.
5. Ragnarsson, L.; Sichen, D. Inclusions Generated during Ingot Casting of Tool Steel. *Steel Res. Int.* **2010**, *81*, 40–47. [[CrossRef](#)]
6. Choi, J.Y.; Lee, H.G.; Kim, J.S. Dissolution rate of Al_2O_3 into molten $\text{CaO-SiO}_2\text{-Al}_2\text{O}_3$ slags. *ISIJ Int.* **2002**, *42*, 852–860. [[CrossRef](#)]
7. Monaghan, B.J.; Nightingale, S.A.; Chen, L.; Brooks, G.A. *VII International Conference on Molten Slags Fluxes and Salts*; Sorlie, M., Ed.; The South African Institute of Mining and Metallurgy: Cape Town, South Africa, 2004.
8. Park, J.S.; Kim, D.H.; Park, J.H. Thermodynamic Stability of Spinel Phase at the Interface between Alumina Refractory and $\text{CaO-CaF}_2\text{-SiO}_2\text{-Al}_2\text{O}_3\text{-MgO-MnO}$ Slags. *J. Am. Ceram. Soc.* **2015**, *98*, 1974–1981. [[CrossRef](#)]

9. Yan, P.C.; Webler, B.A.; Pistorius, P.C.; Fruehan, R.J. Nature of MgO and Al₂O₃ Dissolution in Metallurgical Slags. *Mater. Trans. B* **2015**, *46*, 2414–2418. [[CrossRef](#)]
10. Morris, H.S.; Sawyer, C.; Zhang, Z.T.; Shannon, G.N.; Nakano, J.; Sridhar, S. The interaction of spherical Al₂O₃ particles with molten Al₂O₃-CaO-FeO_x-SiO₂ slags. *Fuel* **2009**, *88*, 670–682. [[CrossRef](#)]
11. Yu, X.; Pomfret, R.J.; Coley, K.S. Dissolution of alumina in mold fluxes. *Mater. Trans. B* **1997**, *28*, 275–279. [[CrossRef](#)]
12. Bui, A.H.; Ha, H.M.; Chung, I.S.; Lee, H.G. Effect of alumina content and solid phase in molten flux on dissolution of alumina. *Met. Mater. Int.* **2005**, *11*, 319–326. [[CrossRef](#)]
13. Frazer, E.J.; Thonstad, J. Alumina Solubility and Diffusion Coefficient of the Dissolved Alumina Species in Low-Temperature Fluoride Electrolytes. *Mater. Trans. B* **2010**, *41*, 543–548. [[CrossRef](#)]
14. Rolseth, S.; Thonstad, J.; Gudbrandsen, H.; Osen, K.S.; Kvello, J.H. On the dissolution of alumina in a low-melting electrolyte for aluminium production. *Aluminium* **2009**, *85*, 52–56.
15. Yang, J.; Graczyk, D.G.; Wunsch, C.; Hryn, J.N. *Light Metals 2007*; Sorlie, M., Ed.; TMS: Warrendale, PA, USA, 2007; pp. 537–541.
16. Monaghan, B.J.; Chen, L. Dissolution behavior of alumina micro-particles in CaO-SiO₂-Al₂O₃ liquid oxide. *J. Non-Cryst. Solids* **2004**, *347*, 254–261. [[CrossRef](#)]
17. Fox, A.; Valdez, M.; Gisby, J.; Atwood, R.; Lee, P.; Sridhar, S. Dissolution of ZrO₂, Al₂O₃, MgO and MgAl₂O₄ Particles in a B₂O₃ Containing Commercial Fluoride-free Mould Slag. *ISIJ Int.* **2004**, *44*, 836–845. [[CrossRef](#)]
18. Verhaeghe, F.; Liu, J.; Guo, M.; Arnout, S.; Blanpain, B.; Wollants, P. Dissolution and diffusion behavior of Al₂O₃ in a CaO-Al₂O₃-SiO₂ liquid: An experimental-numerical approach. *Appl. Phys.* **2007**, *91*, 124104. [[CrossRef](#)]
19. Liu, J.F.; Verhaeghe, F.; Guo, M.X.; Blanpain, B.; Wollants, P. In situ observation of the dissolution of spherical alumina particles in CaO-Al₂O₃-SiO₂ melts. *J. Am. Ceram. Soc.* **2007**, *90*, 3818–3824. [[CrossRef](#)]
20. Orrling, C.; Sridhar, S.; Cramb, A.W. In situ observation of the role of alumina particles on the crystallization behavior of slags. *ISIJ Int.* **2000**, *40*, 877–885. [[CrossRef](#)]
21. Sridhar, S.; Cramb, A.W. Kinetics of Al₂O₃ dissolution in CaO-MgO-SiO₂-Al₂O₃ slags: In situ observations and analysis. *Mater. Trans. B* **2000**, *31*, 406–410. [[CrossRef](#)]
22. Eisenhüttenleute, V.D. *Slag Atlas*, 2nd ed.; Verlag Stahleisen GmbH: Düsseldorf, Germany, 1995; pp. 38–39.
23. Cho, W.D.; Fan, P. Diffusional Dissolution of Alumina in Various Steelmaking Slags. *ISIJ Int.* **2004**, *44*, 229–234. [[CrossRef](#)]
24. Bui, A.H.; Ha, H.M.; Kang, Y.B.; Chung, I.S.; Lee, H.G. Dissolution behavior of alumina in mold fluxes for steel continuous casting. *Met. Mater. Int.* **2005**, *11*, 183–190. [[CrossRef](#)]



© 2016 by the authors; licensee MDPI, Basel, Switzerland. This article is an open access article distributed under the terms and conditions of the Creative Commons Attribution (CC-BY) license (<http://creativecommons.org/licenses/by/4.0/>).